Inorganic Chemistry

Article

pubs.acs.org/IC

Trinuclear Manganese Complexes of Unsymmetrical Polypodal Diamino N_3O_3 Ligands with an Unusual $[Mn_3(\mu\text{-}OR)_4]^{5+}$ Triangular Core: Synthesis, Characterization, and Catalase Activity

Gabriela N. Ledesma,[†] Elodie Anxolabéhère-Mallart,[‡] Eric Rivière,[§] Sonia Mallet-Ladeira,[∥] Christelle Hureau,*[,⊥] and Sandra R. Signorella*[,†]

[†]IQUIR (Instituto de Química Rosario), Consejo Nacional de Investigaciones Científicas y Técnicas (CONICET), Facultad de Ciencias Bioquímicas y Farmacéuticas, Universidad Nacional de Rosario, Suipacha 531, S2002LRK Rosario, Argentina

[‡]Laboratoire Electrochimie Moléculaire-UMR CNRS 7591, University of Paris Diderot, Sorbonne Paris Cité15 rue Jean de Baïf, 75251 Paris, Cedex 13, France

[§]ICMMO-UMR 8182, Equipe Chimie Inorganique, Université Paris-Sud, 91405 Orsay, France

[∥]Institut de Chimie de Toulouse, FR 2599, 118 Route de Narbonne, F-31062 Toulouse, France

[⊥]CNRS, LCC (Laboratoire de Chimie de Coordination) and UPS, INPT, LCC, Université de Toulouse, 205 route de Narbonne, F-31077 Toulouse, France

Supporting Information

ABSTRACT: Two new tri-Mn^{III} complexes of general formula $[Mn_3L_2(\mu\text{-}OH)(OAc)]ClO_4$ (H_3L = 1-[*N*-(2-pyridylmethyl),*N*-(2-hydroxybenzyl)amino]-3-[*N*′-(2-hydroxybenzyl),*N*′-(4-X-benzyl)amino]propan-2-ol; $\mathbf{1}ClO_4$, X = Me; $\mathbf{2}ClO_4$, X = H) have been prepared and characterized. X-ray diffraction analysis of $\mathbf{1}ClO_4$ reveals that the complex cation possesses a $Mn_3(\mu\text{-alkoxo})_2(\mu\text{-hydroxo})(\mu\text{-phenoxo})^{4+}$ core, with the three Mn atoms bound to two fully deprotonated N_3O_3 chelating L^{3-}, one exogenous acetato ligand, and one hydroxo bridge, the structure of which is retained upon dissolution in acetonitrile or methanol. The three Mn atoms occupy the vertices of a nearly isosceles triangle (Mn1···Mn3 = 3.6374(12) Å, Mn2···Mn3 3.5583(13) Å, and Mn1···Mn2 3.2400(12) Å), with one substitution-labile site on the apical Mn ion occupied by terminally bound monodentate acetate. Temperature-dependent magnetic susceptibility studies indicate the presence of predominant antiferromagnetic intramolecular interactions between Mn^{III} ions in $\mathbf{1}ClO_4$. Complexes $\mathbf{1}ClO_4$ and $\mathbf{2}ClO_4$ decompose H_2O_2 at comparable rates upon initial binding of peroxide through acetate substitution, with retention of core structure during catalysis. Kinetic and spectroscopic studies suggest that these complexes employ the $[Mn-(\mu\text{-oxo/aquo})-Mn]^{4+}$ moiety to activate peroxide, with the additional (μ-alkoxo)(μ-phenoxo)Mn(μ-alkoxo) metallobridge carrying out a structural function.

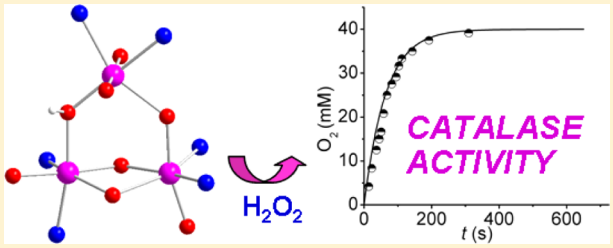

1. INTRODUCTION

Control of structural arrangements and oxidation states of metal ions in multinuclear metal complexes continues to attract interest in the development of metal-based materials. Designing of oligonuclear manganese compounds stems from the recognition of oligonuclear manganese centers in several redox enzymes like Photosystem II (PSII) found in green plants[1] and catalases.[2] Aimed at obtaining functional mimics of these enzymes, great efforts have been made in attempts to correlate the structural characteristics of polynuclear manganese complexes to their chemical properties.[3−6]

A number of polydentate diamino and diimino ligands with a central bridging alcohol group have been used to access complexes containing di- and tetranuclear manganese clusters.[3,5,7] Even when unsymmetrical structures in the polynucleating environment are of crucial importance to modulate the reactivity of each metal center,[8] most used ligands are symmetrical and afford synthetic models with pairs of chemically equivalent manganese ions. Among them, symmetrical polydentate ligands derived from 1,3-diamino-2-propanol and terminal N/O-donor sites ($R^1R^2NCH_2CH(OH)CH_2NR^1R^2$) afford mono-[6,9−12] and bis-alkoxo-bridged[6,13] dinuclear and tetranuclear complexes with $[Mn_4(\mu\text{-}O)_2]^{(6-8)+}$,[14,15] $[Mn_4(\mu_3\text{-}O)_2]^{8+}$,[16] and $[Mn_4(\mu\text{-}OMe)_2]^{8+}$[17] cores, all with paired Mn ions. However, there is no precedent for manganese complexes with unsymmetrical ligands of the type $R^1R^2NCH_2CH(OH)CH_2NR^3R^4$. We wanted to explore the possibility of generating unsymmetrically ligated manganese clusters using this kind of ligands. To achieve this goal, we employed two hexadentate N_3O_3 ligands: 1-[*N*-(2-pyridylmethyl),*N*-(2-hydroxybenzyl)amino]-3-[*N*′-(2-hydroxybenzyl),*N*′-

Received: November 13, 2013
Published: February 17, 2014

   dx.doi.org/10.1021/ic402843y | *Inorg. Chem.* 2014, 53, 2545−2553

Scheme 1. Preparation of the Trinuclear Manganese Complexes 1 (R = Me) and 2 (R = H)

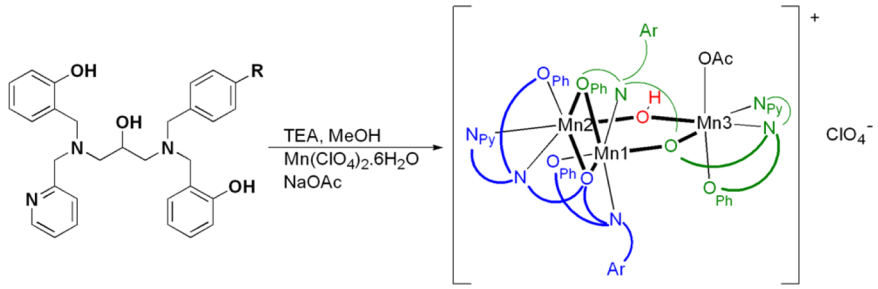

(4-methylbenzyl)amino]propan-2-ol (H_3L^1) and 1-[*N*-(2-pyridylmethyl),*N*-(2-hydroxybenzyl)amino]-3-[*N*′-(2-hydroxybenzyl),*N*′-(benzyl)amino]propan-2-ol (H_3L^2) (Scheme 1).[18] In basic medium, H_3L^{1-2} led to complexes with a triangular $[Mn_3(\mu\text{-OR})_4]^{5+}$ core topology distinctly different from the $[Mn_3(\mu_3\text{-O})]^{(6/7)+}$ oxo-centered triangular geometry found in many Mn_3 compounds.[3,19−22] The synthesis, structure, redox properties, and catalase-like activity of two trinuclear complexes, $[Mn_3L^{1-2}{}_2(\mu\text{-OH})(OAc)]ClO_4$ (L^1, $\mathbf{1}ClO_4$; L^2, $\mathbf{2}ClO_4$), obtained with these ligands are described in this work.

2. EXPERIMENTAL SECTION

2.1. Materials. All reagents were used as purchased without further purification. Ligands H_3L^1 and H_3L^2 were prepared as previously described.[18] Solvents were purified by standard methods.

2.2. Synthesis of the Complexes. *2.2.1. $[Mn_3L^1{}_2(\mu\text{-OH})(OAc)]ClO_4{\cdot}4H_2O$ ($\mathbf{1}ClO_4{\cdot}4H_2O$).* To a solution of H_3L^1 (0.130 g; 0.26 mmol) in methanol (1.5 mL) was added neat triethylamine (0.120 mL; 0.85 mmol). Later, solid $Mn(ClO_4)_2{\cdot}6H_2O$ (0.135 g; 0.53 mmol) was added, and the reaction mixture was stirred at room temperature for 2 h. Then, a solution of sodium acetate (0.355g; 2.6 mmol) in methanol (1.0 mL) was added, and the reaction mixture left to stir for 8 h. The solvent was partially removed under reduced pressure, and the brown precipitate was collected by filtration, washed with water and diethyl ether, and dried over P_2O_5. Yield: 0.216 g (0.15 mmol, 86%). Anal. Calcd for $C_{64}ClMn_3H_{68}N_6O_{13}{\cdot}4H_2O$: C, 54.8; H, 5.5; Mn, 11.8; N, 6.0. Found: C, 54.6; H, 5.1; Mn, 10.9; N, 6.1. ESI-MS: m/z = 1229.3 $[Mn_3L^1{}_2(OH)(OAc)]^+$. Significant IR bands (KBr, ν cm^{-1}): 3434, 3058, 2924, 1595, 1569, 1478, 1453, 1268, 1084, 882, 759, 621, 567, 410. UV−vis λ_{max} nm (ε, M^{-1} cm^{-1}) in CH_3CN 210 (18 730), 270 (9070), 360 (7310), 497 (4785), 634 (1950); in MeOH 330 (7630), 380 (5010), 495 (2575). Single brown crystals of $[Mn_3L^1{}_2(\mu\text{-OH})(OAc)]ClO_4{\cdot}1.5CH_3CN$ ($\mathbf{1}ClO_4{\cdot}1.5CH_3CN$) suitable for X-ray diffraction were obtained from hexane vapor diffusion into a CH_3CN solution of $\mathbf{1}ClO_4{\cdot}4H_2O$.

2.2.2. $[Mn_3L^2{}_2(\mu\text{-OH})(OAc)]ClO_4{\cdot}8H_2O$ ($\mathbf{2}ClO_4{\cdot}8H_2O$). To a solution of H_3L^2 (0.038g; 0.079 mmol) in methanol (2.0 mL) was added neat triethylamine (36 μL; 0.25 mmol). Then, solid $Mn(ClO_4)_2{\cdot}6H_2O$ (0.042 g; 0.165 mmol) was added, and the solution turned deep brown immediately. After stirring at room temperature for 2 h, a solution of sodium acetate (0.115 g; 0.84 mmol) in methanol (0.5 mL) was added to the mixture and left to stir for 4 h. The solvent was partially removed under reduced pressure, and the brown precipitate was collected by filtration, washed with water and diethyl ether, and dried over P_2O_5. Yield: 0.043 g (0.030 mmol, 38%). Anal. Calcd for $C_{62}ClH_{64}Mn_3N_6O_{13}{\cdot}8H_2O$: C, 51.5; H, 5.6; Mn, 11.4; N, 5.8. Found: C, 51.1; H, 4.9; Mn, 12.1; N, 5.9. Significant IR bands (KBr, ν cm^{-1}): 3435, 3059, 2924, 1595, 1567, 1477, 1452, 1265, 1085, 881, 753, 621. UV−vis λ_{max} nm (ε, M^{-1} cm^{-1}) in CH_3CN 210 (22 000), 280 (10 600), 390 (6840), 472 (3350), 580 (1540); in MeOH 380 (8200), 470 (3160).

2.3. Analytical and Physical Measurements. Infrared spectra were recorded on a Perkin-Elmer Spectrum One FT-IR spectrophotometer. Optical spectra were recorded on a Jasco V-550 UV−visible spectrophotometer with thermostatted cell compartments. ESI-mass spectra were carried out with a Q-TRAP AB SCIEX instrument, employing ∼10^{-5} M solutions of the complexes, in methanol or acetonitrile. Cyclic voltammetry was recorded with an Autolab PGSTAT20 potentiostat. The counter electrode was a Pt wire, the reference electrode was a Calomel electrode isolated in a fritted bridge, and the working electrode was a glassy carbon disk. Studies were carried out under Ar, in dry acetonitrile solutions using 0.1 M tetrabutylammonium hexafluorophosphate ($TBAPF_6$) as a supporting electrolyte. Temperature was regulated with a Julabo circulation bath. The working electrode was carefully polished before each voltammogram with a 1 μm diamond paste, sonicated in an ethanol bath, washed carefully with ethanol, and dried with compressed air. Magnetic susceptibility data (2.0−300 K) were collected on powdered samples with a Quantum Design MPMS SQUID susceptometer under an applied magnetic field of 0.5 T. The powder sample was pressed in a pellet to avoid preferential orientations with the magnetic field. All data were corrected for the contribution of the sample holder and diamagnetism of the samples estimated from Pascal's constants.[23]

2.4. Crystallographic Data Collection and Structure Determination. Crystallographic data for compound $[Mn_3L^1{}_2(\mu\text{-OH})(OAc)]ClO_4{\cdot}1.5CH_3CN$ ($\mathbf{1}ClO_4{\cdot}1.5CH_3CN$) were collected at 180(2) K on an Bruker Kappa APEX II Quazar Diffractometer, using a 30 W air-cooled microfocus source with Mo Kα radiation (λ = 0.71073 Å) and equipped with an Oxford Cryosystems Cryostream cooler device. Unit cell determination, data collection, and reduction were carried out using the Bruker APEX2 package and associated integration program SAINT.[24] The structure was solved by direct methods with SHELXS-97 and refined by full-matrix least-squares on F^2 data with SHELXL-97[25] using anisotropic displacement parameters for non-hydrogen atoms. Molecular plots were drawn using the ORTEP program,[26] with 50% probability displacement ellipsoids. Crystal data collection and refinement parameters are summarized in Table 1.

2.5. Catalytic Activity Determination. The catalase-like activity of the complexes was tested by volumetric determination of molecular oxygen evolved after addition of H_2O_2 to a solution of the complex in acetonitrile or methanol. A vial flask capped with a rubber septum, containing a degassed solution of the complex, was thermostatted at 20 °C and connected through a cannula to a gas-measuring buret (precision of 0.1 mL). A solution of H_2O_2 ($[H_2O_2]$:[complex] ratio in the range 100−200:1) was injected through the septum to the stirred complex solution, and the resulting volume of oxygen was measured with the buret.

3. RESULTS AND DISCUSSION

3.1. Syntheses of Complexes $[Mn_3L^{1-2}{}_2(\mu\text{-OH})(OAc)]ClO_4$. Diamines H_3L^{1-2} can act as dinucleating ligands through the central alkoxo bridge. Besides, asymmetry provides these ligands with two chemically different adjacent coordination chambers with N_2O_2 and NO_2 donor sets. Thus, the use of these ligands was conceived as a convenient strategy to induce asymmetrical vacant or labile sites for reactivity of dinuclear manganese complexes. However, treatment of H_3L^{1-2} with 2 equiv of $Mn(ClO_4)_2$ in basic medium afforded trinuclear Mn_3 complexes (instead of the expected dinuclear ones) isolated as

dx.doi.org/10.1021/ic402843y | Inorg. Chem. 2014, 53, 2545−2553

Table 1. Summary of Crystal Data for $1ClO_4 \cdot 1.5CH_3CN$

empirical formula	$C_{64}ClH_{68}Mn_3N_6O_{13} \cdot 1.5(C_2H_3N)$
M	1391.09
temp.	180(2) K
wavelength	0.71073 Å
cryst syst, space group	monoclinic, $C2/c$
unit cell dimens	a = 29.7225(15) Å, α = 90°
	b = 26.7796(14) Å, β = 125.972(2)°
	c = 20.8404(11) Å, γ = 90°
V	13424.8(13) Å^3
Z, ρ_{calcd}	8, 1.377 Mg/m^3
μ_{Mo}	0.663 mm^{-1}
$F(000)$	5784
cryst size	0.12 × 0.08 × 0.04 mm
θ range for data collection	1.14–25.35°
limiting indices	$-35 \le h \le 35$, $-32 \le k \le 32$, $-25 \le l \le 25$
reflns collected/unique	90 924/11 103 [R(int) = 0.1234]
completeness to θ = 25.35	90.3%
max and min transmission	0.9749 and 0.9380
refinement method	full-matrix least-squares on F^2
data/restraints/parameters	11 103/372/959
goodness-of-fit on F^2	1.019
final R indices [$I > 2\sigma(I)$]	R_1 = 0.0690, wR_2 = 0.1787
R indices (all data)	R_1 = 0.1509, wR_2 = 0.2253
largest diff. peak and hole	0.949 and −0.569 e Å^{-3}

$[Mn_3L^{1-}{}_2(\mu\text{-OH})(OAc)]ClO_4$ ($1ClO_4$ and $2ClO_4$) after addition of NaOAc.

Complexation occurs immediately after mixing the Mn^{II} salt with the deprotonated ligand, as evidenced by the observed change of color of the reaction mixture. In the absence of base, no color changes were observed. Therefore, the base facilitates formation of Mn^{III} and deprotonation of the ligand for coordination to the metal.[27−29] It must be stressed that use of $Mn(OAc)_3$ or $MnCl_2$ (the last followed by addition of NaOAc) or NaMeO instead of Et_3N also led to the trinuclear complexes.

3.2. Crystal Structure of $[Mn_3L^1{}_2(\mu\text{-OH})(OAc)]ClO_4 \cdot 1.5CH_3CN$ ($1ClO_4 \cdot 1.5CH_3CN$). Compound $1ClO_4 \cdot 1.5CH_3CN$ crystallizes in the $C2/c$ space group with the asymmetric unit containing a trinuclear complex cation, one perchlorate anion, and one and a half acetonitrile solvent molecules. The molecular structure of complex cation 1^+ is illustrated in Figure 1. In the complex, the three Mn atoms are six coordinated and bound to two fully deprotonated $L^{1(3-)}$ acting as hexadentate chelating ligands through the N_3O_3 donor set and exogenous terminal acetato and bridging hydroxo ligands.

The three manganese atoms in 1^+ occupy the vertices of a nearly isosceles triangle (Mn1···Mn3 = 3.6374(12) Å, Mn3···Mn2 = 3.5583(13) Å, and Mn1···Mn2 = 3.2400(12) Å). One of the Mn atoms (Mn3) is linked to the other two (Mn2 and Mn1) by single μ-hydroxo (O7) and μ-alkoxo (O4, from one ligand) bridges, respectively. Mn1 and Mn2 are doubly bridged by a μ-alkoxo (O1) and μ-phenoxo (O5) from the two ligands defining a Mn_2O_2 unit with angles Mn(2)−O(1)−Mn(1) = 114.33(19)°, Mn(2)−O(5)−Mn(1) = 96.81(15)°, O(1)−Mn(1)−O(5) = 72.12(15)°, and O(1)−Mn(2)−O(5) = 75.04(15)°. The O4 and O7 atoms are coplanar with the three Mn centers (O4 and O7 are displaced slightly out of the plane defined by the three Mn ions, by 0.096 and 0.002 Å, respectively), while the segment defined by O1 and O5 of the

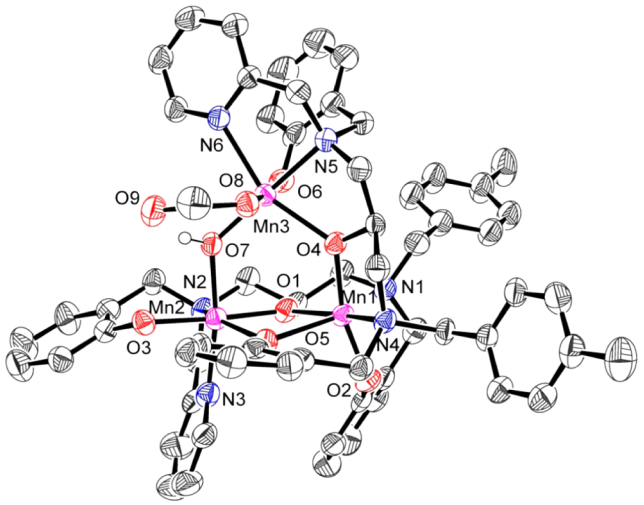

Figure 1. ORTEP drawing of $[Mn_3L^1{}_2(\mu\text{-OH})(OAc)]^+$ (1^+). Hydrogen atoms are omitted for clarity except the one on O7.

(μ-alkoxo)(μ-phenoxo) double bridge forms an angle of 85.83° with the Mn1O4Mn3O7Mn2 plane. The Mn_2(μ-alkoxo)(μ-phenoxo) moiety is also almost planar with a dihedral angle between the planes Mn1O1O5 and Mn2O1O5 equal to 168.07° and between Mn1O1Mn2 and Mn1O5Mn2 planes of 163.91°. A schematic picture of the Mn_3 core is shown in Figure 2, and relevant bond lengths are collected in Table 2.

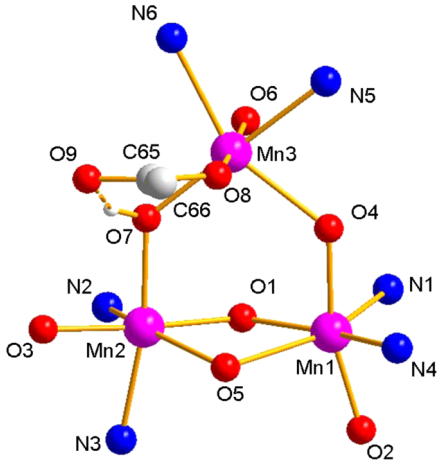

Figure 2. Schematic representation of the trinuclear core of 1^+.

Table 2. Selected Bond Lengths for Compound $1ClO_4 \cdot 1.5CH_3CN$ (Angstroms)

Mn1−O1	1.965(4)	Mn2−N3	2.110(5)
Mn1−O2	1.851(4)	Mn3−N5	2.148(5)
Mn1−O4	1.906(4)	Mn3−N6	2.263(5)
Mn1−O5	2.199(4)	Mn3−O4	2.138(4)
Mn1−N1	2.447(5)	Mn3−O6	1.878(4)
Mn1−N4	2.108(5)	Mn3−O7	1.923(4)
Mn2−O1	1.890(4)	Mn3−O8	1.932(4)
Mn2−O3	1.849(4)	Mn1···Mn2	3.2400(12)
Mn2−O5	2.134(4)	Mn1···Mn3	3.6374(12)
Mn2−O7	1.978(4)	Mn2···Mn3	3.5583(13)
Mn2−N2	2.228(5)		

dx.doi.org/10.1021/ic402843y | Inorg. Chem. 2014, 53, 2545−2553

The hydroxo bridging anion and terminal acetato are associated through the H bond, as shown by the O7−H···O9 (OAc) short contact in Figure 2, with distances O7−H 0.835 Å and H···O9 (OAc) 2.055 Å.

All Mn atoms are six coordinate with distorted octahedral geometry and N_2O_4 first coordination sphere. Charge balance considerations, bond valence sum (BVS) calculation[30] (Table S1, Supporting Information), and inspection of the metric parameters indicate that the complex can be best described as Mn^{III}_3. The three Mn^{III} ions exhibit Jahn−Teller axial elongation, as expected for high-spin d^4 ions in the distorted octahedral geometry, with Jahn−Teller axes O5−Mn1−N1 (Mn1−O/N_{av} 2.32 Å), O5−Mn2−N2 (Mn2−O/N_{av} 2.17 Å), and O4−Mn3−N6 (Mn3−O/N_{av} 2.20 Å) being remarkably longer than those on the other two axes of each octahedron (Mn−O/N_{av} 1.96 Å). The lack of signal in the EPR spectrum, the magnetic behavior (see below), and the intense stretching band at 3435 cm^{-1} observed in the IR spectrum of crystals of $1ClO_4 \cdot 1.5CH_3CN$ (Figure 3), corresponding to the bridging OH group, also support charge assignments.

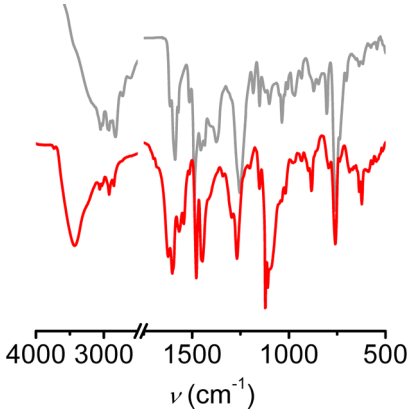

Figure 3. FT-IR spectra of free ligand H_3L^1 (gray line) and $1ClO_4$ (crystals, red line).

To our knowledge, this geometrical motif for the Mn_3 unit had only been observed in triangular oxo-bridged manganese clusters containing the $[Mn^{IV}_3O_4]^{4+}$ core.[3,31] $Mn^{II}Mn^{III}_2$ and Mn^{III}_3 complexes usually contain an oxo-centered triangular $[Mn_3(\mu_3\text{-}O)]^{6/7+}$ [3,21,22,31,32] or $[Mn_3(\mu_3\text{-}OMe)]^{8+}$,[33] as well as linear or bent open trinuclear units.[3,34−36]

Recently, a trinuclear $Mn^{II}_3(\mu\text{-}OR)_3$ complex with a chairlike structural motif has been successfully employed to access the $[Mn_3CaO_4]^{6+}$ core as a model for the Mn_3Ca subsite of the OEC in PSII.[37,38] In line with this, the trimetallic $[Mn_3(\mu\text{-}OR)_4]^{5+}$ structure of $\mathbf{1}^+$ can be envisaged as a precursor for synthesis of the heterometallic tetranuclear core through incorporation of Ca to the Mn_3 core via the acetate bridge, thus highlighting the interest in this unique and peculiar structural unit.

3.3. IR Spectroscopy. The IR spectra of $\mathbf{1}ClO_4$ (powder and crystals) and $\mathbf{2}ClO_4$ evidence the "fingerprint" pattern of the ligand coordinated to the Mn ions and support the analogous structures of both compounds (Figure S1, Supporting Information). The two complexes exhibit strong phenoxo and pyridyl ring absorptions in the region of 1595−1560 cm^{-1}, which are shifted from the values observed in the free ligands (~11 cm^{-1}) as a consequence of coordination to the metal and absorption peaks at 1605 and 1450 cm^{-1} assigned to the antisymmetrical and symmetrical stretching vibrations of terminally bound acetate (shown for $\mathbf{1}ClO_4$ in Figure 3).[39,40] In the IR spectra of the free ligands, the O−H in-plane bending vibration occurs at 1375 cm^{-1}; this peak is absent in the spectra of $\mathbf{1}ClO_4$ and $\mathbf{2}ClO_4$, indicating that phenol groups are deprotonated in these complexes. Compounds $\mathbf{1}ClO_4$ and $\mathbf{2}ClO_4$ (powdered samples and crystals) show a peak at 3400 cm^{-1} corresponding to the O−H stretching vibration of the hydroxo bridge. Powdered samples of the two complexes exhibit additional broad bands at ~3500 cm^{-1} assigned to noncoordinated water molecules. In addition, both complexes display two peaks at 1085 and 621 cm^{-1} corresponding to the antisymmetrical stretching and bending vibration modes of noncoordinated tetrahedral ClO_4^- ion.

3.4. Magnetic Properties. Magnetic susceptibility was measured under a 0.5 T field in the 2−300 K temperature range on a powder sample of complex $\mathbf{1}ClO_4$. As shown in Figure 4, the $\chi_M T$ value of $\mathbf{1}ClO_4$ is 7.73 cm^3 K mol^{-1} at 300 K, which is less than the spin-only limit for three noninteracting Mn^{III}

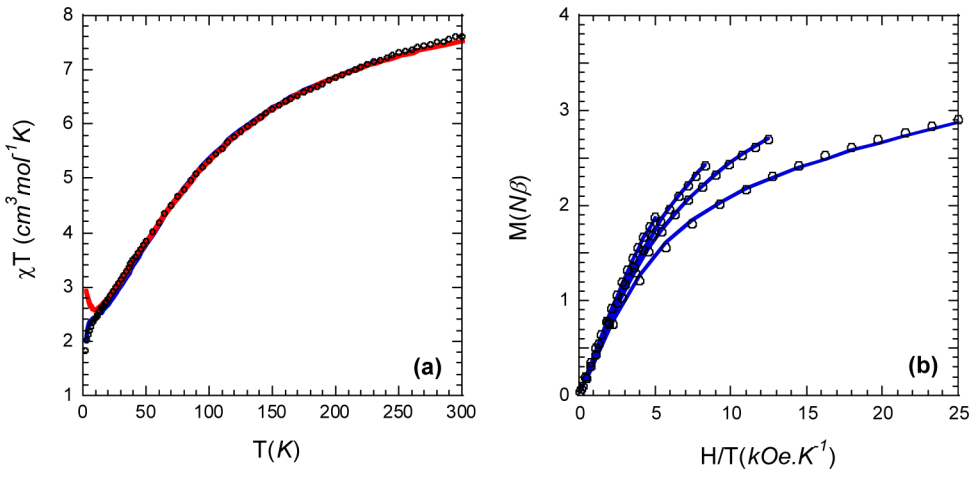

Figure 4. (a) Temperature dependence of $\chi_M T$ for compound $1ClO_4$: (O) experimental data, solid line in red shows the simulation obtained with the isotropic Hamiltonian (fitting in the range 300−50 K), solid line in blue corresponds to the best fit including a local zero-field splitting parameter D (fitting in the range 300−2 K). (b) Magnetization vs H/T curves recorded at 2, 4, 6, and 10 K. Solid lines correspond to the curves determined using the parameters deduced from the $\chi_M T = f(T)$ curve.

dx.doi.org/10.1021/ic402843y | Inorg. Chem. 2014, 53, 2545−2553

($\chi_M T$ = 9.00 cm^3 K mol^{-1}, assuming an isotropic g value of 2.00). When lowering the temperature, the $\chi_M T$ product continuously decreases from 7.73 to 2.8 cm^3 K mol^{-1} at 10.0 K and then more rapidly to 2.02. The observed behavior suggests the presence of antiferromagnetic exchange interactions in the trinuclear complex leading to an S = 2 spin ground state. The decrease at low temperature (T < 10 K) could arise from intermolecular antiferromagnetic interactions or zero-field splitting.

The magnetic behavior of the compound was first analyzed using the isotropic spin Hamiltonian $H = -2J(S_1S_2) - 2J'(S_1S_3 + S_2S_3)$. Despite the presence of three different types of bridges, the similarity of Mn1···Mn3 and Mn2···Mn3 distances allows the use of only two exchange pathways: the first (J) through the μ-alkoxo and μ-phenoxo bridges and the second (J') through the μ-hydroxo or the μ-alkoxo bridge. To avoid intermolecular interactions or zero-field splitting influence, experimental data were fitted in the temperature range from 300 to 50 K. The least-squares fitting[41,42] of experimental data gives J = −9.3 cm^{-1}, J' = −2.5 cm^{-1}, and g = 2.01 ($R = 2 \times 10^{-5}$).[42] The associated spin ladder shows that the ground state is S = 2 separated by only 3 cm^{-1} from the first excited state S = 1. In Figure 4a, the red line represents the simulation resulting from these best-fit parameters. At low temperature, the simulated curve deviates strongly from the experimental data. To improve the reproduction of the lowering of $\chi_M T$ below 10 K, a local axial magnetic anisotropy parameter D was introduced. The best fit of experimental data (solid blue line in Figure 4a) was obtained with D = −3.5 cm^{-1}, J = −8.5 cm^{-1}, J' = −2.8 cm^{-1}, and g = 2.01 ($R = 1.3 \times 10^{-4}$).

The variation of the magnetization with the applied field was recorded at 2, 4, 6, and 10 K; the data are reported in the form of magnetization vs the ratio of the field to temperature in Figure 4b. The experimental data are satisfactory reproduced using the parameters deduced from the $\chi_M T = f(T)$ fitting process (solid lines). The magnitude of the D value found for Mn^{III} is consistent with values reported in the literature.

Unlike some others metals (copper complexes for example[43]) magneto-structural correlation is not clearly established for manganese complexes. Recent works try to summarize all the parameters which govern the interactions in Mn^{III} dimers[44,45] or in trinuclear compounds.[46,47]

It is admitted that the relative orientation of the Jahn−Teller axes of Mn^{III} has a major influence on the sign and strength of the exchange; in such a way Berg[44] classified bis-μ-alkoxo dimers into three types: (i) if the axes are colinear and perpendicular to the plane of the bridge the interaction is weakly antiferromagnetic, (ii) if the Jahn−Teller axes are parallel to each other and parallel to the plane of the bridge the interaction is very weak and can be antiferromagnetic or ferromagnetic, (iii) if the Jahn−Teller axes are perpendicular to each other (one in the bridging plane and the other perpendicular to the bridging plane) the coupling is ferromagnetic. It is always difficult to transpose results from dinuclear to trinuclear compounds. Here, the μ-alkoxo and μ-phenoxo bridges in **1**ClO$_4$ cannot be assigned to one of the types defined by Berg as the Jahn−Teller axis of Mn1 and Mn2 are in the plane of the bridge but are not parallel to each other. Nevertheless, other magneto-structural correlations have been found. For instance, they are based on the angle Mn−O−Mn or the distance Mn−O. For **1**ClO$_4$, the relative strength between J and J' can be explained by the number of bridges as it has been shown that the antiferromagnetic coupling increases with the number of bridges.[45] Likewise, the antiferromagnetic coupling decreases with increasing of the angle Mn−O−Mn or the average of the Mn−O distance increases. The angles Mn1O1Mn2 (114.39°) or Mn1O5Mn2 (96.83°) are much more acute than Mn1O4Mn3 (127.98°) or Mn2O7Mn3 (131.56°), favoring the antiferromagnetic exchange through the μ-alkoxo and μ-phenoxo bridges between Mn1 and Mn2 atoms. The influence of Mn−O distances is less clear as the average distance in the μ-phenoxo bridge is the longest (2.166 Å), a value which would lead to a ferromagnetic coupling.[44]

3.5. Solution Studies. *3.5.1. ESI-MS and Electronic Spectroscopy.* ESI-mass spectra of complexes **1**ClO$_4$ and **2**ClO$_4$ confirm their chemical composition and retention of nuclearity in solution. In CH$_3$CN, the positive mode ESI mass spectrum of complex **1**ClO$_4$ (Figure S2, Supporting Information) shows three main peaks at m/z = 1229.3 (15%), 1169.3 (100%), and 572.2 (35.8%), which originate from the $[Mn_3L^1{}_2(\mu\text{-OH})(OAc)]^+$, $[Mn_3L^1{}_2(\mu\text{-O})]^+$ (corresponding to the loss of AcOH), and $[MnL^1Na]^+$ monocations, respectively. The last two species are most likely to be generated within the spectrometer during electrospray. In the case of complex **2**ClO$_4$, either in MeOH or in CH$_3$CN (Figures S3, Supporting Information and 8), the higher mass region of the spectra is dominated by the peak at m/z 1141.3 ($[Mn_3L^2{}_2(\mu\text{-O})]^+$). The isotopic pattern distribution of the major peaks of both complexes matches their calculated spectra very well (see Figures S2 and S3, Supporting Information).

The electronic spectra of complexes **1**ClO$_4$ and **2**ClO$_4$ recorded in CH$_3$CN exhibit an intense absorption at 210 nm, attributed to $\pi \rightarrow \pi^*$ transitions from the ligands and ligand-to-metal charge transfer (LMCT) transitions from the phenoxo to Mn^{III} in the region 350−550 nm, also observed for a variety of Mn^{III} complexes with phenoxo ligands (Figure 5).[48−52]

The broad band observed as a shoulder around 600 nm is associated to d−d transitions.[12,49,50,53,54] After isolation of the d−d band from the LMCT band, a value of 750 M^{-1} cm^{-1} can be estimated for the ε value, which is consistent with the presence of three Mn^{III} ions per mole of complex.[12,52,53] In methanol, the intense LMCT band at ∼500 nm obscures the d−d transitions (Figures S4 and S5, Supporting Information). In the two solvents, spectra of the complexes registered at different time lengths (during 7 h) after preparation of solutions showed identical λ_{max} and molar absorbance coefficients, indicating that **1**ClO$_4$ and **2**ClO$_4$ are stable in these solvents.

3.5.2. Electrochemical Studies. Cyclic voltammetry of complexes **1**ClO$_4$ and **2**ClO$_4$ was studied at a glassy carbon electrode in CH$_3$CN (Figure 6 and Figure S6, Supporting Information). The cyclic voltammogram of **1**ClO$_4$ (see Figure 6a) exhibits a quasi-reversible (one electron) cathodic process (1) at E^0 (1) = −0.185 V vs SCE (ΔE_p = 148 mV at a scan rate of 0.1 V s^{-1}) followed by a broader irreversible peak (2) at $E_c{}^2$ = −0.760 V vs SCE. These two processes are attributed to successive reduction of the Mn^{III} ions in the cation **1**$^+$. The E^0 (1) value fits with the ones reported for the Mn^{III}Mn^{III}/Mn^{II}Mn^{III} reduction process in dinuclear complexes with a similar N_2O_4 coordination sphere around the Mn^{III} ion.[7,12] The attribution of this first reduction process to Mn1, Mn2, or Mn3 ion is tricky, although the reversibility of the wave and the chemical surroundings of the three Mn ions suggest the attribution to Mn1 or Mn2 over Mn3, the coordination sphere around the latter center containing a labile acetate ion (vide infra). The irreversibility of the second cathodic process

dx.doi.org/10.1021/ic402843y | Inorg. Chem. 2014, 53, 2545−2553

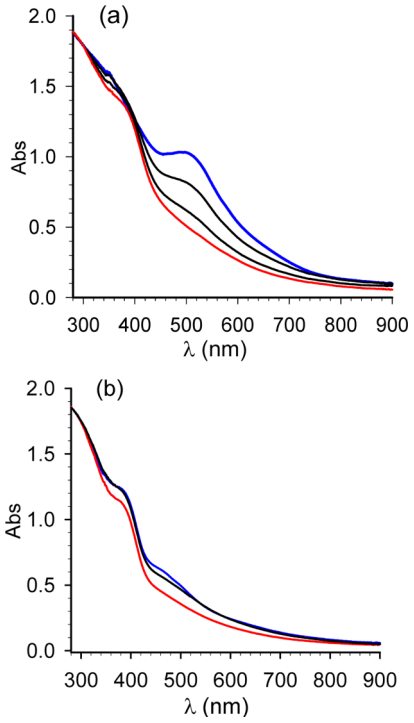

Figure 5. Electronic spectra in CH_3CN, registered (a) before (blue line) and after three successive additions of 200 equiv of H_2O_2 (black and red lines) to a 0.21 mM solution of $\mathbf{1}ClO_4$, (b) before (blue line) and after additions of 100 (black line) and 600 (red line) equiv of H_2O_2 to a 0.18 mM solution of $\mathbf{2}ClO_4$. T = 293 K, l = 1 cm.

indicates that the trinuclear structure is likely modified in the $Mn^{II}Mn^{II}Mn^{III}$ oxidation state.

On oxidation, the cyclic voltammogram of $\mathbf{1}ClO_4$ shows two successive anodic processes (3 and 3′) at E_a^3 = 0.420 V vs SCE (peak 3 showing a plateau shape) and $E_a^{3'}$ = 0.860 V vs SCE (irreversible peak), the first wave being much lower in intensity than the second one. A plausible explanation is that in solution cation $\mathbf{1}^+$ exists in equilibrium with a form in which the acetate exogenous ligand is decoordinated from the $Mn3^{III}$ ion (Scheme 2). The first wave (3) is thus attributed to oxidation of the $Mn3^{III}$ ion in $\mathbf{1}^+$ and the second wave (3′) to oxidation of the $Mn3^{III}$ ion in $\mathbf{1}^+$ for which the acetate ion has been replaced by a solvent molecule. The E^0 (3) = 0.34 V vs SCE value is slightly higher (150 mV) than the one reported for oxidation of dinuclear complexes with N_2O_4 coordination sphere around the Mn^{III} ion (0.19 V vs SCE) for which two of the oxygen atoms

Scheme 2. Square Scheme Showing the Equilibrium of the Two Forms of $\mathbf{1}^+$ In Acetonitrile Solution

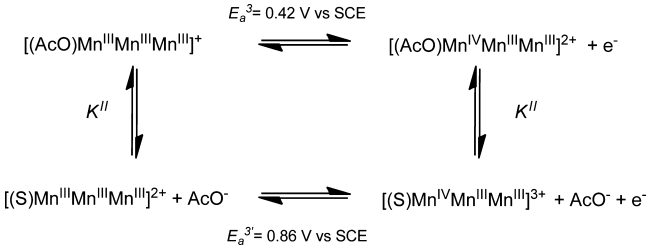

originates from bridging acetato or methoxo ligands.[7] Upon addition of acetate solution the cyclic voltammetry trace of $\mathbf{1}^+$ shows an increase of the intensity and reversibility of the peak at E_a^3 (Figure 6b), thus supporting the attribution of the two peaks at E_a^3 and $E_a^{3'}$. We note that the acetate ion could be substituted by a residual water solvent molecule, which would most likely be deprotonated in the $Mn3^{IV}$ oxidation state. This electrochemical−chemical (EC) mechanism would thus be responsible for the irreversibility of wave 3′ as it has previously been reported in acetonitrile solution.[54−56]

A third anodic reversible wave is observed at 1.06 V vs SCE (ΔE_p = 148 mV at 0.1 V s^{-1}), which is attributed to the Mn^{III} to Mn^{IV} oxidation process of Mn1 or Mn2 ions.

Cyclic voltammetry recorded for cation $\mathbf{2}^+$ in acetonitrile (Figure S6, Supporting Information) displays a behavior similar to cation $\mathbf{1}^+$ with two cathodic peaks at E_c^1 = −0.175 and E_c^2 = −0.700 and two anodic peaks at E_a^3 = 0.505 and $E_a^{3'}$ = 0.962 V vs SCE.

3.5.3. Catalytic Activity Study. Numerous and diverse diMn complexes of binucleating ligands involving either alkoxo or phenoxo bridges have been reported as catalase (CAT) functional models.[6] Kinetic and mechanistic studies have shown that the catalytic activity of these diMn compounds depends on structural factors, such as Mn···Mn distance, bridging motif, ligand flexibility, vacant sites, that, in turn, are key points for controlling the peroxide binding mode.[7] Solution studies show that the structural features of $\mathbf{1}ClO_4$ are retained upon dissolution and that $\mathbf{1}ClO_4$ and $\mathbf{2}ClO_4$ have the same signatures both in CH_3CN and in MeOH (see Figure S7, Supporting Information for the electrochemical fingerprint in MeOH). Thus, compounds $\mathbf{1}ClO_4$ and $\mathbf{2}ClO_4$ possess three potential Mn^{III}_2 moieties to react with H_2O_2: Mn3−μ-hydroxo−Mn2, Mn3−μ-alkoxo−Mn1, and Mn1−μ-alkoxo-μ-phenoxo−Mn2, affording a unique way to compare the CAT

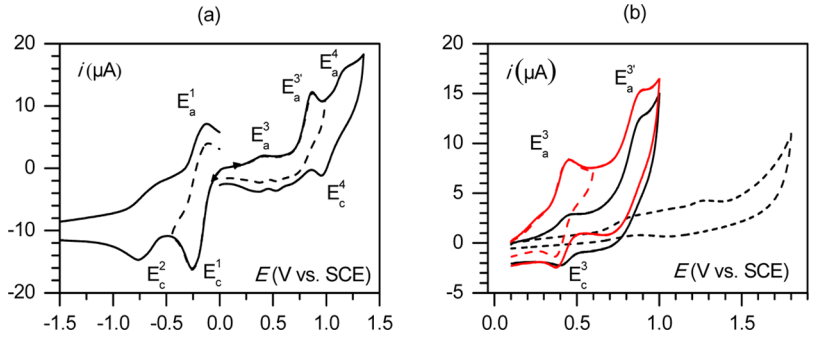

Figure 6. Cyclic voltammetry at 0.1 V s^{-1}, T = 293 K, on glassy carbon electrode in CH_3CN + 0.1 M NBu_4PF_6 of (a) $\mathbf{1}^+$ (0.8 mM) and (b) 0.6 mM tetraethylamonium acetate (dotted black line), $\mathbf{1}^+$ (0.6 mM) (black line), and $\mathbf{1}^+$ (0.6 mM) in the presence of 0.6 mM of tetraethylamonium acetate (red line). E^0 (1) and E^0 (3) are calculated as the mean value of E_a^1 and E_c^1 and E_a^3 and E_c^3, respectively.

dx.doi.org/10.1021/ic402843y | Inorg. Chem. 2014, 53, 2545−2553

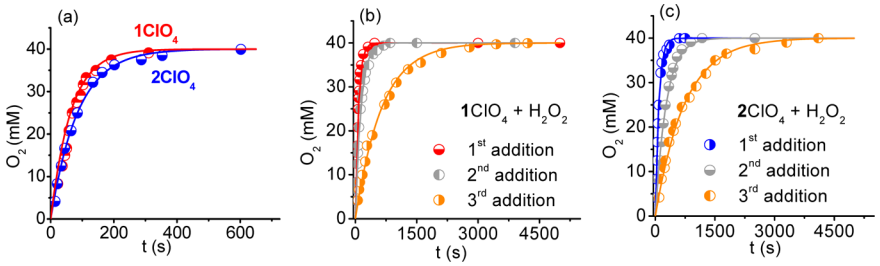

Figure 7. Time dependence of O_2 evolution upon reaction of **1**ClO_4 and **2**ClO_4 with 80 mM H_2O_2 in CH_3CN at 293 K. After one addition of H_2O_2: [**1**ClO_4] = 0.44 mM, r_i = 1.81 s^{-1}; [**2**ClO_4] = 0.42 mM, r_i = 1.76 s^{-1} (a) and after three successive additions of 80 mM H_2O_2 over a 5 mL solution of **1**ClO_4 (b) and **2**ClO_4 (c).

activity of the three bridging motifs and establish the role of the additional metallobridge on the CAT activity. Addition of H_2O_2 to a solution of complexes **1**ClO_4 and **2**ClO_4 in CH_3CN or methanol caused the immediate vigorous evolution of dioxygen coupled to color changes: from brown to orange in CH_3CN and from brown to yellow in methanol. The relative CAT activity of the complexes in these solvents was determined by the volumetric measurement of evolved O_2. As shown in Figure 7a, in CH_3CN, the two complexes disproportionate H_2O_2 at a similar rate.

In this solvent, initial rates vary linearly with $[catalyst]_0$ and $[H_2O_2]_0$ and the two complexes convert more than 600 equiv of H_2O_2 to O_2. Successive additions of excess H_2O_2 to the catalyst solution yielded a stoichiometric amount of O_2 but the initial rate of H_2O_2 dismutation gradually decreased after each new addition (Figure 7b and 7c).

Monitoring of the catalytic reaction of **2**ClO_4 by ESI-MS gave a valuable indication on the nuclearity of the catalyst during the catalytic cycle. The positive ESI-mass spectra of 190:1 H_2O_2:**2**ClO_4 mixtures in CH_3CN, taken during and at the end of the O_2 evolution, are dominated by the peak at m/z = 1141 (corresponding to $([Mn_3L^2{}_2(\mu\text{-O})]^+)$ (Figure 8),

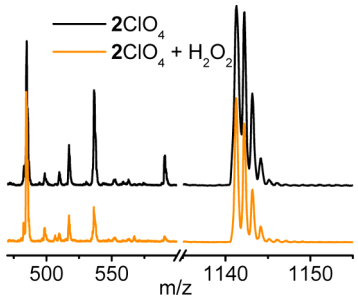

Figure 8. ESI-mass spectra taken before and at the end of the reaction of **2**ClO_4 with 190 equiv of H_2O_2 in CH_3CN.

providing a clear indication that the Mn^{III}_3 core persists during H_2O_2 disproportionation. This was confirmed by UV–vis spectra taken at the end of O_2 evolution, which shows that the initial spectral pattern of the complexes is retained. However, after each new H_2O_2 addition, the intensity of the LMCT absorption bands decreased (Figure 5), as did the peaks of the starting complex in the ESI-mass spectra, denoting gradual loss of catalyst. Consequently, after successive additions of excess H_2O_2, the rate of O_2 evolution diminished (Figure 7b and 7c) as the [catalyst] in the reaction mixture decreased. For the two complexes, the lack of a lag period and the first-order dependence of reaction on catalyst imply that the starting complex is the true catalyst or it converts into the active form upon fast reaction with H_2O_2.

In methanol, complexes **1**ClO_4 and **2**ClO_4 disproportionate H_2O_2 with initial rates r_i = 1.48 and 1.51 s^{-1}, respectively, using the same conditions as in CH_3CN. Immediately after addition of a 190:1 excess of H_2O_2 to the methanolic solution of catalyst, the intensity of the LMCT and d–d bands decreased down to 60% of the initial value (shown for complex **1** in Figure S4, Supporting Information). As the reaction progressed, the initial spectral pattern was restored but the intensity was still lower than for the starting complex. After completion of the reaction, absorbance had reached 85% of the initial value (Figure S4, Supporting Information). These absorption changes occurred with an isosbestic point at 622 nm, suggesting rapid conversion of the initial complex into the reduced form of the catalyst during reaction, which then reoxidizes slowly, as observed for diMn complexes of 1,3-bis[(2-hydroxybenzyl)(2-pyridylmethyl)amino]propan-2-ol,[7] 1,3-bis(salicylideneamino)-propan-2-ol,[57] and *N,N,N′,N′*-tetrakis(2-methylenebenzimidazolyl)-1,3-diaminopropan-2-ol,[58] which cycle between Mn^{II}_2/Mn^{III}_2 oxidation states and for which oxidation of the catalyst is the slow turnover-limiting step (peroxide reduction) in the reaction. A second addition of a 190:1 excess of H_2O_2 over catalyst evolved O_2 at essentially the same initial rate (Figure S8, Supporting Information).

A possible mechanism including an active trinuclear Mn^{III} $[Mn_3L^{1-2}{}_2(\mu\text{-O})]^+$ species is presented in Scheme 3. It is proposed that initial reaction of H_2O_2 with the starting complex yields AcOH, O_2, and the two-electron-reduced active form of catalyst $[Mn_3L^{1-2}{}_2(\mu\text{-OH}_2)]^+$. Binding of peroxide to the starting complex might take place through an acetate shift with the endogenous μ-hydroxo ligand acting as internal base to assist deprotonation of the terminally bound HO_2^- coupled to its two-electron oxidation, without a change in the total formal charge of the catalyst. The so-formed $Mn^{II}_2Mn^{III}$ complex participates in the slow reductive half-reaction (turnover-limiting step) to yield the oxidized active form of the catalyst: $[Mn_3L^{1-2}{}_2(\mu\text{-O})]^+$ and water. The oxidized Mn^{III}_3 catalyst reacts with another H_2O_2 molecule in the fast oxidative half-reaction to yield O_2 and restore $[Mn_3L^{1-2}{}_2(\mu\text{-OH}_2)]^+$, thus closing the cycle. Binding of H_2O_2 to $[Mn_3L^{1-2}{}_2(\mu\text{-O})]^+$ might occur at the vacant coordination site on Mn3 coupled to proton transfer to the oxo bridge. This mechanistic scheme is fully consistent with the kinetic and spectroscopic studies of H_2O_2 disproportionation by complexes **1**ClO_4 and **2**ClO_4.

Initial rates of H_2O_2 disproportionation by complexes **1**ClO_4 and **2**ClO_4 are in the same range as for diMn complexes of alkoxo-bridging ligands, which in turn are much higher than for complexes with phenoxo-bridged diMn cores (Table 3). In

dx.doi.org/10.1021/ic402843y | Inorg. Chem. 2014, 53, 2545–2553

Scheme 3. Proposed Catalytic Cycle for the H_2O_2 Disproportionation by Complexes $1ClO_4$ and $2ClO_4$

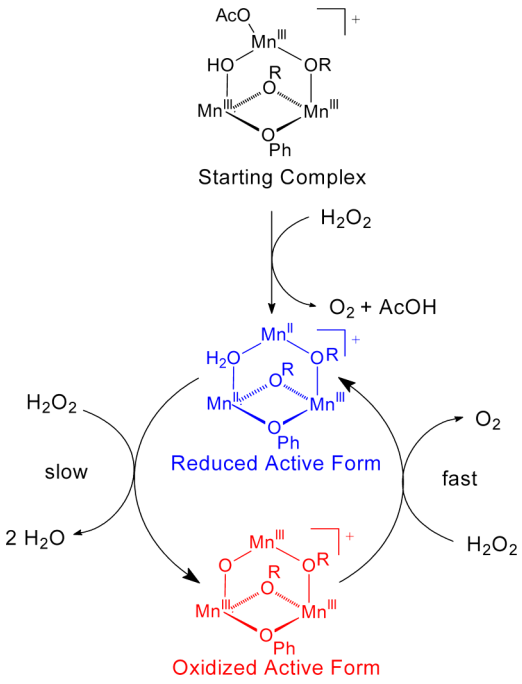

particular, the catalytic behavior of complexes $1ClO_4$ and $2ClO_4$ closely resembles that of $[Mn_2(\mu\text{-OAc})(\mu\text{-OH}_2)(benzimpnO)]^{2+}$ (Table 3, entry 4), which has an intermetallic distance similar to Mn3···Mn2(Mn1), binds peroxide as a terminal ligand through acetate shift, and uses an oxidized oxo-bridged Mn^{III}_2 species in the catalytic cycle.[58] The present complexes should employ the Mn3−μ-oxo/aquo−Mn2 moiety to activate peroxide, with the additional bridges (Mn3−μ-alkoxo−Mn1 and Mn1−μ-alkoxo-μ-phenoxo−Mn2) contributing to stabilize the metal cluster. The last is particularly evident in methanol, a protic solvent where μ-alkoxo/oxo-diMn complexes inactivate after a few cycles except if an exogenous base is added.[58,62]

4. CONCLUDING REMARKS

Unsymmetrical H_3L^{1-2} ligands yield a new type of trinuclear Mn complexes with a core structure that is distinctly different from those seen before with symmetrical ligands derived of 1,3-diaminopropan-2-ol. The resulting Mn complexes are stable in solution and react with hydrogen peroxide employing the Mn3−μ-oxo/aquo−Mn2 moiety, with the additional metallobridges carrying out a structural function. Interestingly, the catalytic $[Mn_3L^{1-2}_2(\mu\text{-O})]^+$ core resists conditions employed in the CAT test in methanol, a protic solvent where most diMn complexes lose activity by metal dissociation. On the basis of their triangular $[Mn_3(\mu\text{-OR})_4]^{5+}$ core structure and robustness, the trinuclear core of these compounds can be envisaged as precursor of the heterometallic tetranuclear $[Mn_3CaO_4]^{6+}$ subsite of the oxygen-evolving center of PSII. This highlights the interest in the use of the present unsymmetrical ligands in the synthesis of manganese complexes with a unique and peculiar structural core.

■ ASSOCIATED CONTENT

Supporting Information

Crystallographic data in CIF format; IR spectra of $1ClO_4$ and $2ClO_4$; ESI-mass spectra and simulated isotopic distribution pattern of $1ClO_4$ and $2ClO_4$; UV−vis spectra for $1ClO_4$ + H_2O_2 in MeOH and $2ClO_4$ in MeOH; cyclic voltammetry of $2ClO_4$ in acetonitrile solution and $1ClO_4$ and $2ClO_4$ in MeOH; O_2 evolution curves for $1ClO_4$ + H_2O_2 in MeOH. This material is available free of charge via the Internet at http://pubs.acs.org.

■ AUTHOR INFORMATION

Corresponding Authors

*E-mail: Christelle.Hureau@lcc-toulouse.fr.
*E-mail: signorella@iquir-conicet.gov.ar.

Notes

The authors declare no competing financial interest.

■ ACKNOWLEDGMENTS

We thank the National University of Rosario and CONICET for financial support and CONICET-CNRS for a bilateral agreement (Res. 991/2013). G.N.L. thanks the B. Houssay Program from CONICET (Argentine) and MEST/MAEE (France) for a postdoctoral fellowship.

■ REFERENCES

(1) Ferreira, K. N.; Iverson, T. M.; Maghlaoui, K.; Barber, J.; Iwata, S. *Science* **2004**, *303*, 1831−1838.
(2) Barynin, V. V.; Whittaker, M. M.; Antonyuk, S. V.; Lamzin, V. S.; Harrison, P. M.; Artymiuk, P. J.; Whittaker, J. W. *Structure* **2001**, *9*, 725−738.
(3) Mukhopadhyay, S.; Mandal, S. K.; Bhaduri, S.; Armstrong, W. H. *Chem. Rev.* **2004**, *104*, 3981−4026.
(4) McEvoy, J. P.; Brudvig, G. W. *Chem. Rev.* **2006**, *106*, 4455−4483.

Table 3. Rates of H_2O_2 Disproportionation by Complexes $1ClO_4$ and $2ClO_4$ and Comparison with Other CAT Mimics

	catalyst	r_i (mM H_2O_2 mM cat^{-1} s^{-1})[a]	endogenous ligand bridge	Mn···Mn (Å)	ref
1	1^+−2^+	1.76−1.81	hydroxo/alkoxo	3.56/3.64	this work
			alkoxo−phenoxo	3.24	
2	$[Mn_2(\mu\text{-OAc})_2(hppnO)]^+$	0.95	alkoxo	3.2	7
3	$[Mn(X\text{-salpnO})]_2$	4.1−9.1	bis-alkoxo	3.2−3.3	57
4	$[Mn_2(\mu\text{-OAc})(\mu\text{-OH}_2)(benzimpnO)]^{2+}$	2.6	alkoxo	3.54[b]	58
5	$[Mn_2(bprol\text{-}^tBu\text{-}p)(\mu\text{-OAc})(H_2O)_2]^{2+}$	0.023	phenoxo	3.25	59
6	$[Mn_2(X\text{-bphba})_2Cl_2]$	0.014	bis-phenoxo	3.39−3.49	60
7	$[Mn_2(etsalim)_4(Hetsalim)_2]_2$	0.031	bis-phenoxo	3.37	61

[a] r_i values were calculated from reported kinetic parameters. $[H_2O_2]$ = 0.08 M, [catalyst] = 0.42 mM. [b] Mn−Mn distance of the reduced Mn^{II}_2 form. hppnOH: 1,3-bis[(2-hydroxybenzyl)(2-pyridylmethyl)amino]propan-2-ol. salpnOH: 1,3-bis(salicylideneamino)propan-2-ol. benzimpnOH: *N*,*N*,*N*′,*N*′-tetrakis(2-methylenebenzimidazolyl)-1,3-diaminopropan-2-ol. $H_3bprol\text{-}^tBu\text{-}p$: 2,6-bis(prolin-1-yl)methyl-4-*tert*-butylphenol. bphba: 2-{(*N*,*N*-bis(2-pyridylmethyl) amino)methyl}phenol. Hetsalim: ethyl salicylimidate.

dx.doi.org/10.1021/ic402843y | *Inorg. Chem.* 2014, 53, 2545−2553

(5) Mullins, C. S.; Pecoraro, V. L. *Coord. Chem. Rev.* **2008**, *252*, 416−443.
(6) Wu, A. J.; Penner-Hahn, J. E.; Pecoraro, V. L. *Chem. Rev.* **2004**, *104*, 903−938.
(7) Signorella, S.; Hureau, C. *Coord. Chem. Rev.* **2012**, *256*, 1229−1245.
(8) Belle, C.; Pierre, J. L. *Eur. J. Inorg. Chem.* **2003**, 4137−4146.
(9) Berben, L. A.; Peters, J. C. *Inorg. Chem.* **2008**, *47*, 11669−11679.
(10) Jung, M.; Sharma, A.; Hinderberger, D.; Braun, S.; Schatzschneider, U.; Rentschler, E. *Eur. J. Inorg. Chem.* **2009**, 1495−1502.
(11) Boelrijk, A. E. M.; Khangulov, S. V.; Dismukes, G. C. *Inorg. Chem.* **2000**, *39*, 3009−3019.
(12) Signorella, S.; Tuchagues, J.-P.; Moreno, D.; Palopoli, C. In *Inorganic Biochemistry Research Progress*; Hughes, J. G., Robinson, A. J., Eds.; Nova. Sci. Publ. Inc.: New York, 2008; pp 243−279.
(13) Gelasco, A.; Kirk, M. L.; Kampf, J. W.; Pecoraro, V. L. *Inorg. Chem.* **1997**, *36*, 1829−1837.
(14) Mikata, Y.; Wakamatsu, M.; So, H.; Abe, Y.; Mikuriya, M.; Fukui, K.; Yano, S. *Inorg. Chem.* **2005**, *44*, 7268−7270.
(15) Mukhopadhyay, S.; Mok, H. J.; Staples, R. J.; Armstrong, W. H. *J. Am. Chem. Soc.* **2004**, *126*, 9202−9204.
(16) Bagai, R.; Abboud, K. A.; Christou, G. *Dalton Trans.* **2006**, 3306−3312.
(17) Lan, Y.; Novitchi, G.; Clérac, R.; Tang, J. K.; Madhu, N. T.; Hewitt, I. J.; Anson, C. E.; Brooker, S.; Powell, A. K. *Dalton Trans.* **2009**, 1721−1727.
(18) Ledesma, G.; Signorella, S. *Tetrahedron Lett.* **2012**, *53*, 5699−5702.
(19) Baca, S. G.; Stoeckli-Evans, H.; Ambrus, C.; Malinovskii, S. T.; Malaestean, I.; Gerbeleu, N.; Decurtins, S. *Polyhedron* **2006**, *25*, 3617−3627.
(20) Viciano-Chumillas, M.; Tanase, S.; Mutikainen, I.; Turpeinen, U.; de Jongh, L. J.; Reedijk, J. *Inorg. Chem.* **2008**, *47*, 5919−5929.
(21) Lampropoulos, C.; Abboud, K. A.; Stamatatos, T. C.; Christou, G. *Inorg. Chem.* **2009**, *48*, 813−815.
(22) Yang, C. I.; Cheng, K. H.; Hung, S. P.; Nakano, M.; Tsai, H. L. *Polyhedron* **2011**, *30*, 3272−3278.
(23) Pascal, P. *Ann. Chim. Phys.* **1910**, *19*, 5−70.
(24) Bruker. *APEX2 and SAINT*; Bruker AXS Inc.: Madison, WI, 2008.
(25) Sheldrick, G. M. *Acta Crystallogr.* **2008**, *A64*, 112−122.
(26) Farrugia, L. J. *J. Appl. Crystallogr.* **2012**, *45*, 849−854.
(27) Moreno, D.; Daier, V.; Palopoli, C.; Tuchagues, J. P.; Signorella, S. *J. Inorg. Biochem.* **2010**, *104*, 496−502.
(28) Gohdes, J. W.; Armstrong, W. H. *Inorg. Chem.* **1992**, *31*, 368−373.
(29) Shyu, H.; Wei, H.; Wang, Y. *Inorg. Chim. Acta* **1999**, *290*, 8−13.
(30) Liu, W.; Thorp, H. H. *Inorg. Chem.* **1993**, *32*, 4102−4105.
(31) Baffert, C.; Orio, M.; Pantazis, D. A.; Duboc, C.; Blackman, A. G.; Blondin, G.; Neese, F.; Deronzier, A.; Collomb, M. N. *Inorg. Chem.* **2009**, *48*, 10281−10288.
(32) Cañada-Vilalta, C.; Streib, W. E.; Huffman, J. C.; O'Brien, T. A.; Davidson, E. R.; Christou, G. *Inorg. Chem.* **2004**, *43*, 101−115.
(33) Liu, C. M.; Zhang, D. Q.; Zhu, D.-B. *Dalton Trans.* **2010**, *39*, 1781−1785.
(34) Dimitrakopoulou, A.; Psycharis, V.; Raptopoulou, C. P.; Terzis, A.; Tangoulis, V.; Kessissoglou, D. P. *Inorg. Chem.* **2008**, *47*, 7608−7614.
(35) Hureau, C.; Anxolabéhère-Mallart, E.; Blondin, G.; Rivière, E.; Nierlich, M. *Eur. J. Inorg. Chem.* **2005**, 4808−4817.
(36) Mandal, D.; Chatterjee, P. B.; Bhattacharya, S.; Choi, K.-Y.; Clérac, R.; Chaudhury, M. *Inorg. Chem.* **2009**, *48*, 1826−1835.
(37) Tsui, E. Y.; Kanady, J. S.; Day, M. W.; Agapie, T. *Chem. Commun.* **2011**, *47*, 4189−4191.
(38) Kanady, J. S.; Tsui, E. Y.; Day, M. W.; Agapie, T. *Science* **2011**, *333*, 733−736.
(39) Nakamoto, K. *Infrared and Raman Spectra of Inorganic and Coordination Compounds*, 5th ed.; Wiley Interscience: New York, 1997.
(40) Deacon, G. B.; Phillips, R. J. *Coord. Chem. Rev.* **1980**, *33*, 227−250.
(41) A minimization routine was added to MAGPACK package: Borra's-Almenar, J. J.; Clemente-Juan, J. M.; Coronado, E.; Tsukerblat, B. S. *J. Comput. Chem.* **2001**, *22*, 985−991. Borras-Almenar, J. J.; Clemente-Juan, J. M.; Coronado, E.; Tsukerblat, B. S. *Inorg. Chem.* **1999**, *38*, 6081−6088.
(42) $R = [\Sigma(\chi T_{exp} - \chi T_{calcd})^2]/[\Sigma(\chi T_{calcd})^2]$.
(43) Ruiz, E.; Alvarez, S.; Rodriguez-Fortea, A.; Alemany, P.; Pouillon, Y.; Massobrio, C. *Magnetism: Molecules to Materials II*; Wiley-VCH Verlag GmbH & Co.: Weinheim, Germany, 2001; p 227.
(44) Berg, N.; Rajeskumar, T.; Taylor, S. M.; Brechin, E. K.; Rajaraman, G.; Jones, L. F. *Chem. Eur. J.* **2012**, *18*, 5906−5918.
(45) Pantazis, D. A.; Krewald, V.; Orio, M.; Neese, F. *Dalton Trans.* **2010**, *39*, 4959−4967.
(46) Cano, J.; Cauchy, T.; Ruiz, E.; Milios, C. J.; Stoumpos, C. C.; Stamatatos, T. C.; Perlepes, S.; Christou, G.; Brechin, E. K. *Dalton Trans.* **2008**, 234−240.
(47) Zhang, Y.-Q.; Luo, C.-L. *Dalton Trans.* **2009**, 5627−5636.
(48) Dubois, L.; Xiang, D. F.; Tan, S. S.; Pecaut, J.; Jones, P.; Baudron, S.; Le Pape, L.; Latour, J. M.; Baffer, C.; Chardon-Noblat, S.; Collomb, M. N.; Deronzier, A. *Inorg. Chem.* **2003**, *42*, 750−760.
(49) Karsten, P.; Neves, A.; Bortoluzzi, A.; Strähle, J.; Maichle-Mössmer, C. *Inorg. Chem. Commun.* **2002**, *5*, 434−438.
(50) Neves, A.; Erthal, S. M. D.; Vencato, I.; Ceccato, A. S.; Mascarehas, Y. P.; Nascimento, O. R.; Hörner, M.; Batista, A. A. *Inorg. Chem.* **1992**, *31*, 4749−4755.
(51) Hirotsu, M.; Kojima, M.; Mori, W.; Yoshikawa, Y. *Bull. Chem. Soc. Jpn.* **1998**, *71*, 2873−2884.
(52) Biava, H.; Palopoli, C.; Duhayon, C.; Tuchagues, J. P.; Signorella, S. *Inorg. Chem.* **2009**, *48*, 3205−3214.
(53) Hureau, C.; Anxolabéhère-Mallart, E.; Nierlich, M.; Gonnet, F.; Rivière, E.; Blondin, G. *Eur. J. Inorg. Chem.* **2002**, 2710−2719.
(54) Hureau, C.; Sabater, L.; Anxolabéhère-Mallart, E.; Nierlich, M.; Charlot, M.-F.; Gonnet, F.; Rivière, E.; Blondin, G. *Chem. Eur. J.* **2004**, *10*, 1998−2010.
(55) Groni, S.; Hureau, C.; Guillot, R.; Blondin, G.; Blain, G.; Anxolabéhère-Mallart, E. *Inorg.Chem.* **2008**, *47*, 11783−11797.
(56) Hureau, C.; Blondin, G.; Charlot, M.-F.; Philouze, C.; Nierlich, M.; Césario, M.; Anxolabéhère-Mallart, E. *Inorg. Chem.* **2005**, *44*, 3669−3683.
(57) Gelasco, A.; Bensiek, S.; Pecoraro, V. L. *Inorg. Chem.* **1998**, *37*, 3301−3309.
(58) Boelrijk, A. E. M.; Dismukes, G. C. *Inorg. Chem.* **2000**, *39*, 3020−3028.
(59) Kaizer, J.; Csonka, R.; Speier, G. *React. Kinet. Catal. Lett.* **2008**, *94*, 157−163.
(60) Reddig, N.; Pursche, D.; Kloskowski, M.; Slinn, C.; Baldeau, S. M.; Rompel, A. *Eur. J. Inorg. Chem.* **2004**, 879−887.
(61) Godbole, M. D.; Kloskowski, M.; Hage, R.; Rompel, A.; Mills, A. M.; Spek, A. L.; Bouwman, E. *Eur. J. Inorg. Chem.* **2005**, 305−313.
(62) Palopoli, C.; Bruzzo, N.; Hureau, C.; Ladeira, S.; Murgida, D.; Signorella, S. *Inorg. Chem.* **2011**, *50*, 8973−8983.